CrystEngComm RSCPublishing

PAPER

Compositionally Tunable $Cu_2Sn(S_xSe_{1-x})_3$ Nanocrystals: Facile Direct Solution-phase Synthesis, Characterization, and Scalable Procedure

Cite this: DOI: 10.1039/x0xx00000x

Received 00th January 2013, Accepted 00th January 2013

DOI: 10.1039/x0xx00000x

www.rsc.org/

Qingshuang Liang[1, 2], Lin Han[1, 2], Xiaolong Deng[1, 2], Chuangang Yao[1, 2], Junling Meng[1, 2], Xiaojuan Liu[1*], Jian Meng[1*]

In this paper, we report a facile, low-cost synthesis of $Cu_2Sn(S_xSe_{1-x})_3$ colloidal nanocrystals (NCs) by heating a mixture of metal salts, sulfur powder, selenium powder, oleylamine and dodecanethiol. The composition of the $Cu_2Sn(S_xSe_{1-x})_3$ NCs could be tuned across the x range from 0 to1 by modulating the S/Se precursors molar ratio. The lattice parameters (a and c) of the $Cu_2Sn(S_xSe_{1-x})_3$ NCs, calculated from X-ray diffraction patterns, were consistent with Vegard's law, confirming the formation of homogeneous nanocrystals. The X-ray diffraction and transmission electron microscopy results indicated that the as-prepared $Cu_2Sn(S_xSe_{1-x})_3$ NCs had the monoclinic structure. The UV-visible absorption spectra of the $Cu_2Sn(S_xSe_{1-x})_3$ NCs revealed that the band gap of the nanocrystals could be tailored from 1.55 to 1.87 eV by decreasing the Se content. Additionally, as compared with the more commonly used hot injection method, the procedure developed here is highly suitable for large-scale colloidal nanocrystal production, which we tested by performing a gram-scale synthesis.

Introduction

The need to develop low-cost, scalable and solution-processable photovoltaic material is a leading impetus for the research in the field of semiconductor nanocrystal synthesis. Though $Cu(In,Ga)Se_2$ system compounds have been well-known as promising candidates for solar energy harvesting material,[1, 2] the limited supply and increasing price of indium and gallium has made the large-scale, cost-effective production of these materials hardly realized.[3] Recently, there is a growing interest in the development of Cu_2ZnSnS_4 and $Cu_2ZnSnSe_4$ nanocrystals.[4-9] In the benefit of their earth-abundant constituents, optimal band gap, and high absorption coefficient, these Cu-based multicomponent semiconductors have been expected to be substitutes for the $Cu(In,Ga)Se_2$ materials.[10, 11] Yet due to the difficulty of the composition and phase control of the Cu_2ZnSnX_4 (X=S or Se) compounds,[8] another potential substitute materials, simpler compound systems such as Cu_2SnS_3 and Cu_2SnSe_3, have drawn a great attention recently.[12-20] Cu_2SnS_3 is a ternary semiconductor with a p-type direct band gap of 0.95-1.35 eV in bulk material, while Cu_2SnSe_3 has a p-type direct band gap in the range of 0.8-1.1 eV.[12, 17] Both of them possess high absorption coefficient and high electron and hole mobility. Cu_2SnS_3-based solar cells have been fabricated and demonstrated solar energy conversion efficiency of 2.84%.[18]

Meanwhile, multicomponent semiconductor nanocrystals are of great interest in the manufacture of thin-film solar cells.[5, 6, 21-23] Multicomponent NCs offer the advantage of having tunable structural, optical, electronic, and defect properties that all can influence the photovoltaic properties. Multicomponent NCs synthesized by alloying two constituent may not only inherit the properties of their parent materials but also exhibit new properties distinct from them. It has been reported that a large efficiency increase appeared when an amount of Se is incorporated into the Cu_2ZnSnS_4 nanocrystal thin film.[5] However, it still remains a big challenge to obtain stoichionmetric multicomponent semiconductor NCs.[23-28] The difficulty to control the reactivity of each precursor in the multicomponent system usually results in unwanted side products.

Besides, as mentioned elsewhere,[10, 21, 29] the creation of nanostructured suspension ink for use in a scalable coating process is a key step in the development of low-cost thin-film solar cells. The use of colloidal nanocrystal inks requires manufacturing of large amounts of NC materials, which calls for large-scale synthesis processes. To date, various synthesis approaches have been developed to prepare semiconductor nanocrystals, such as the hot-injection approach and the synthesis by direct heating of mixtures of precursors.[30-32] The hot-injection route, relying on a fast injection of precursors to induce nucleation and growth, is not an ideal option for large-scale synthesis.[33, 34] Large efforts have been dedicated to the direct heating procedures.[26, 35, 36] Chiang et al. have reported a facile heating-up synthesis of quaternary $CuIn(S_{1-x}Se_x)_2$ nanocrystals recently. Manna and co-workers have synthesized composition and band gap tunable $CuIn_xGa_{1-x}S_2$ nanocrystals via a phosphine-free and scalable procedure. Based on inexpensive, environmentally friendly reagents, a one-spot fast direct solution-phase synthesis approach is highly attractive and applicable for the fabrication of photovoltaic absorber material.

In the present work, we report a facile and up-scalable synthesis of colloidal $Cu_2Sn(S_xSe_{1-x})_3$ NCs by heating commercial metal salts (CuCl, $SnBr_2$) in a chalcogen solution containing oleylamine and 1-dodecanethiol. Nanocrystals with controlled composition ranging from Cu_2SnS_3 to Cu_2SnSe_3 through intermediate $Cu_2Sn(S_xSe_{1-x})_3$ with tunable x, could be achieved by tailoring the precursor molar ratios. The as-prepared $Cu_2Sn(S_xSe_{1-x})_3$ NCs possess good trends in their lattice parameter and band gap variations when they are modulated by their x-values. A crystallochemical study using X-ray diffraction and transmission electron microscopy revealed that the as-prepared $Cu_2Sn(S_xSe_{1-x})_3$ NCs have the monoclinic structure. Furthermore, the feasibility of up-scaling for this approach is demonstrated by performing a gram-scale synthesis of $Cu_2Sn(S_{0.5}Se_{0.5})_3$ NCs.

Experimental Section

Chemicals

All chemicals were used as received without further purification. Tin (II) bromide ($SnBr_2$, 99%) was obtained from Sigma-Aldrich. Copper (I) chloride (CuCl, 97%) was purchased from Alfa Aesar. Cupric acetate ($Cu(OAc)_2$, 99%), selenium powder (99.999%), sulfur powder (99.99%), and 1-dodecanethiol (98%), oleylamine (80-90%) were obtained from Aladdin. Hexane (analytical reagent), ethanol (analytical reagent) were purchased from Beijing chemical works.

Synthesis of $Cu_2Sn(S_xSe_{1-x})_3$ nanocrystals

The synthesis of $Cu_2Sn(S_xSe_{1-x})_3$ nanocrystals was carried out in oleylamine (OAm) solution by a facile one-pot method. In a typical synthesis, 0.5 mmol $SnBr_2$(0.1392 g), 1 mmol CuCl (0.099 g), 0.75 mmol selenium powder(0.0592 g) and 0.75 mmol sulfur powder(0.024 g) were loaded to a 100 ml three-neck flask attached with a Schlenk line. Then, 10 mL of OAm and 1 mL of 1-dodecanethiol (DDT) were added. The mixed solution was degassed at 130 °C for 1 h with stirring and purged with argon three times. The temperature was then slowly raised to 240 °C with a ramping rate of 2 °C/min. The reaction was held at 240 °C for 1 h with continuous vigorous stirring. After the mixture was cooled to room temperature, 5 mL of hexane and 25 mL of ethanol were added, and the mixture was sonicated for 5 min to remove all the free ligands and the unreacted precursors. The solution was centrifuged at 9000 rpm for 10 min. The upper layer liquid was decanted, and the isolated solid was dispersed in hexane and reprecipitated by adding enthol. The centrifugation and precipitation procedure was repeated three times and the final products were redispersed in hexane or dried under vacuum for further measurements.

For gram-scale production of $Cu_2Sn(S_{0.5}Se_{0.5})_3$ NCs, the synthesis was carried out by dissolving 10 mmol $Cu(OAc)_2$ (1.8164 g), 5 mmol $SnBr_2$ (1.392 g), 7.5 mmol Se (0.5922 g) and 7.5 mmol S (0.24 g) to the solution of 60 mL oleylamine and 6 mL 1-dodecanethiol, degassing under vacuum for 1 h at 130 °C, then heating to 240 °C and keeping at this temperature for 1 h. The resulting product was cooled to room temperature and cleaned three times as described above, and the final NCs were dried under vacuum for further measurements.

Thin films for optoelectronic properties characterizations were deposited by spin-casting nanocrystals dispersed in toluene. The fabrication details of the device structure are as follows: an patterned indium tin oxide (ITO)-coated glass was used as the substrate and cleaned by successive ultrasonic treatment in acetone and isopropyl alcohol and then dried at 120 °C for 30 min. The ITO glass was then subjected to UV-Ozone treatment for 10 min. The Cu_2Sn $(S_{0.5}Se_{0.5})_3$ film was fabricated by spin-casting the concentrated nanocrystals toluene dispersion on the substrate. The substrates were then transferred into an evaporator and pumped down to 4×10^{-4} Pa to deposit 100-nm-thick aluminum (Al) cathodes. Post thermal annealing was carried out at 140 °C for 3 min on a hot plate inside a nitrogen-filled glovebox and the devices were encapsulated for measurement.

Characterization

UV-visible absorption spectra was recorded on a Cary 50 Scan UV-visible spectrophotometer (Varian, USA). X-ray power diffraction (XRD) patterns were recorded on a D8 Focus diffractometer (Bruker) with a Cu Kα1 radiation source (λ= 0.15406 nm). The composition of the as-prepared $Cu_2Sn(S_xSe_{1-x})_3$ nanocrystals was determined quasi-quantitatively by a Hitachi S-4800 high-resolution FE-SEM equipped with an energy-dispersive X-ray spectroscopy (EDS) analyzer (XP30, Philips), at an acceleration voltage of 20 kV. Transmission electron microscopy (TEM) was performed on a JEOL-100CX electron microscope with an accelerating voltage of 80 kV. The samples for STEM-EDS were prepared by dropping nanocrystals dispersed in ethanol onto nickel grids. Thermogravimetric Analysis (TGA) was carried out using a STA 449 F3 simultaneous thermal analyzer. I–V curves were measured using a computercontrolled Keithley 236 source meter under AM1.5G illumination from a calibrated solar simulator with irradiation intensity of 100 mW/cm^2.

Results and Discussion

The challenge for synthesis of multicomponent semiconductor nanocrystals is the accurate control of their stoichiometry composition. Balancing the reactivity of the relative precursors was found to be the key pathway to producing the desired composition without unwanted side products.[26] Cu^+ ions are very soft Lewis acids, whereas Sn^{4+} ions are hard Lewis acids. According to the principle of hard and soft acids and bases (HSAB), the chalcogen (S,Se) precursors, being as soft Lewis

Table 1. Composition Analysis, Lattice Parameters (a and c), and Band Gap Energies of $Cu_2Sn(S_xSe_{1-x})_3$ Nanocrystals

Target compound	Cu:Sn:S:Se precusor ratio	Cu:Sn:S:Se ratio measured by EDS	a (Å)	c (Å)	E_g(eV)
Cu_2SnSe_3 (x=0)	2:1:0:3	30.84: 15.06: 5.51: 48.58 (2.05:1:0.36:3.22)	6.93	11.89	1.55(1)
$Cu_2Sn(S_{0.2}Se_{0.8})_3$(x=0.2)	2:1:0.375:2.625	31.83: 16.23: 10.03: 41.9 (1.96:1:0.62:2.58)	6.90	11.85	1.59(1)
$Cu_2Sn(S_{0.3}Se_{0.7})_3$(x=0.3)	2:1:0.75:2.25	30.78: 15.95: 17.19: 36.08 (1.93:1:1.07:2.26)	6.86	11.79	1.65(2)
$Cu_2Sn(S_{0.5}Se_{0.5})_3$(x=0.5)	2:1:1.5:1.5	32.81: 16.63: 25.43: 25.12 (1.97:1:1.53:1.51)	6.77	11.74	1.67(2)
$Cu_2Sn(S_{0.7}Se_{0.3})_3$(x=0.7)	2:1:1.875:1.125	34.96: 17.12: 33.54: 14.37 (2.04:1:1.96:0.84)	6.73	11.64	1.75(2)
$Cu_2Sn(S_{0.8}Se_{0.2})_3$(x=0.8)	2:1:2.625:0.375	32.72: 16.61: 39.98: 10.13 (1.97:1:2.41:0.61)	6.67	11.57	1.80(2)
Cu_2SnS_3 (x=1)	2:1:3:0	33.79: 16.93: 49.28:0 (1.99:1:2.91:0)	6.64	11.53	1.87(2)

bases, react preferentially with Cu^+ than Sn^{4+}. When tin bromide and copper chloride were dissolved directly in the pure OAm solution and heated to 240 °C for 1 h in an inert atmosphere, formation of CuS_x (x=1-2), Sn_2S_3 phases was found (Figure S1a, Supporting Information). The different reaction activities of the two cation precursors with anion resulted in a separated nucleus and ultimately phase separation. It has been reported that alkane thiols could suppress the reactivity of the soft Lewis acids effectively.[24] Therefore, dodecanethiol was added to our react systems. When the combination of precursors with desired mole ratio was mixed to the OAm solution with 1 mL DDT, reacted in 240 °C for 1 h, $Cu_2Sn(S_xSn_{1-x})_3$ quaternary nanocrystals with controlled S/Se ratio formed (Figure S1b). We speculated that when dodecanethiol was added to the reaction, the strong binding of DDT and Cu^+ ions gave rise to the relatively slow reaction of the copper ions with chalcogen, and ultimately leading the formation of homogeneous $Cu_2Sn(S_xSe_{1-x})_3$ NCs.

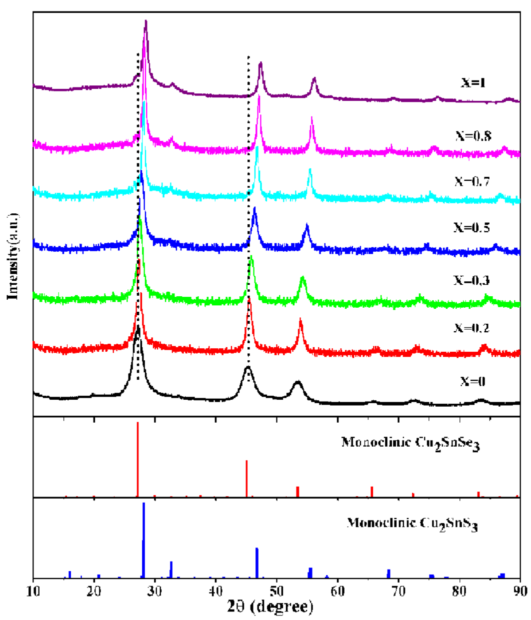

Fig.1 XRD patterns of $Cu_2Sn(S_xSe_{1-x})_3$ nanocrystals for various values of x. The simulated XRD pattern of monoclinic Cu_2SnSe_3 and Cu_2SnS_3 are shown below.

The compositions of the resulting $Cu_2Sn(S_xSe_{1-x})_3$ quaternary nanocrystals were determined by energy-dispersive X-ray spectroscopy (EDS) and the results are listed in Table 1. The Cu:Sn:S:Se mole ratios in the products are in close agreement with the ratios of the precursors. This indicates that the reactivity of the relative precursors was balanced and successful formation of composition tunable $Cu_2Sn(S_xSe_{1-x})_3$ quaternary nanocrystals were achieved.

Figure 1 shows the powder XRD patterns of the $Cu_2Sn(S_xSe_{1-x})_3$ NCs. The major diffraction peak shows a systematic shift to higher angle with decreasing Se contents, which may have ruled out the phase separation or separated nucleation of Cu_2SnS_3 and Cu_2SnSe_3 during the growth of the $Cu_2Sn(S_xSe_{1-x})_3$ NCs. The shift in the diffraction peaks is attributed to the reducing lattice constants due to the substitution of significantly smaller S^{2-} to the larger Se^{2-} in the $Cu_2Sn(S_xSe_{1-x})_3$ lattices. As shown in Figure 2 (a) and (b), the lattice parameters (a and c) of the $Cu_2Sn(S_xSe_{1-x})_3$ NCs have a linear relation with the S composition, which is in agreement with Vegard's law. STEM-EDS elemental mapping of both $Cu_2Sn(S_{0.7}Se_{0.3})_3$ and $Cu_2Sn(S_{0.5}Se_{0.5})_3$ nanocrystals confirmed that Cu, Sn, Se, and S were equally distributed in the NCs (Figure S2, Supporting Information). These results indicate that we have successfully synthesized alloyed NCs with homogeneous distribution of S and Se in the $Cu_2Sn(S_xSe_{1-x})_3$ matrix.

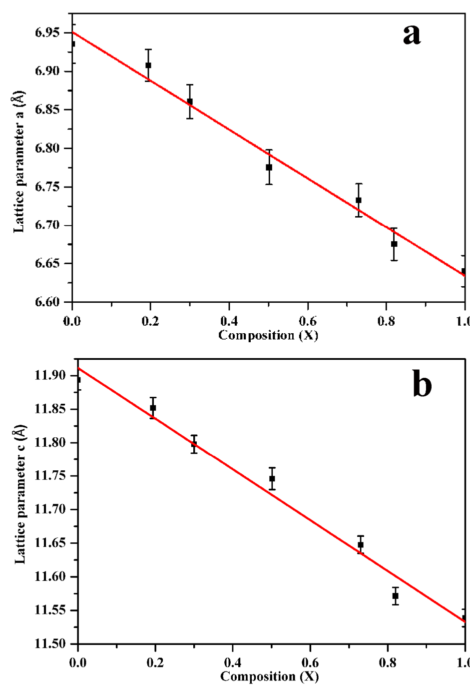

Fig.2 Relationship between the change of (a) lattice parameter a and (b) lattice parameter c with x of $Cu_2Sn(S_xSe_{1-x})_3$ nanocrystals.

In the literatures,[12, 14, 15, 17] various kinds of crystal structures have been reported for Cu_2SnS_3 and Cu_2SnSe_3 ternary compounds, such as $F\bar{4}3m$ cubic, $I\bar{4}2d$ tetragonal and $C1c1$ monoclinic. These crystal phases are quite similar and the difference in these structures exists only in the small superstructure peaks and the splitting of main peaks. To acquire the crystalline structure of the as-prepared $Cu_2Sn(S_xSe_{1-x})_3$ NCs, a close investigation of XRD, high-resolution transmission electron microscopy (HRTEM), and select area electron diffraction (SAED) on the multicomponent $Cu_2Sn(S_xSe_{1-x})_3$ nanocrystals was performed. As shown in Figure 3, the X-ray diffraction pattern of the as-prepared Cu_2SnSe_3 NCs is more fitting with the monoclinic structure, compared with cubic structure. The small peaks at 2θ = 17.22, 19.97, 32.66, 34.33 can be indexed to be the ($\bar{1}11$), (021), (041), ($\bar{1}32$) plane of monoclinic Cu_2SnSe_3, respectively. Figure 4 shows a HRTEM image of the Cu_2SnSe_3 nanocrystals and the corresponding fast-Fourier transform (FFT). The clear lattice fringes for the whole nanocrystal shown in the HRTEM image indicates that these nanoparticles are all well crystalline. The observed d-spacings of 2.00, 3.28, and 1.71 Å are in agreement with the (060), (200), and (260) planes of monoclinic Cu_2SnSe_3, respectively. On the base of the above results, we may possibly conclude that the as-prepared Cu_2SnSe_3 NCs exhibit monoclinic structure. Similarly, the as-synthesized $Cu_2Sn(S_xSe_{1-x})_3$ NCs can also be assigned to the monoclinic phase (Figure S 3-5, Supporting Information).

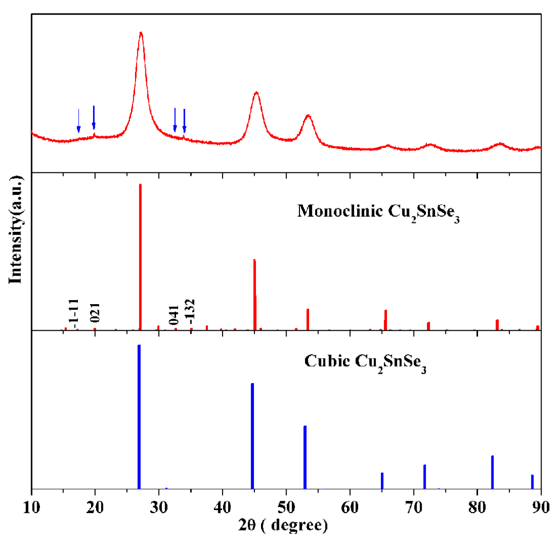

Fig.3 XRD pattern of the as-prepared Cu_2SnSe_3 NCs and simulated XRD pattern of monoclinic and cubic structures.

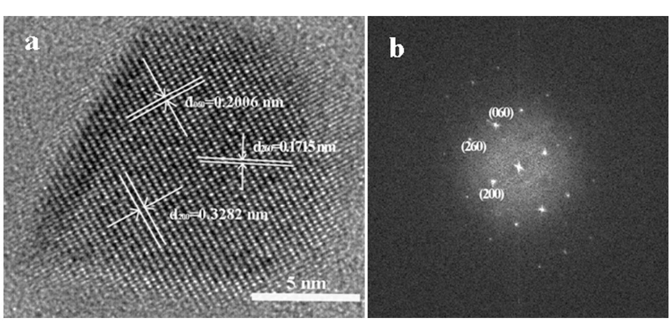

Fig.4 (a) HR-TEM image of a single Cu_2SnSe_3 nonocrystal; (b) The corresponding fast-Fourier transform (FFT) image.

A typical TEM image of $Cu_2Sn(S_xSe_{1-x})_3$ NCs (x=0.7) is shown in Figure 5 (a). The as-prepared nanocrystals were monodispersed and quasi-spherical. Figure 5 (b-h) displays HRTEM images highlighting the lattice fringes of individual $Cu_2Sn(S_xSe_{1-x})_3$ nanocrystals representative of the various compositions. As the Se content decreases, the lattice spacings of $d_{(200)}$ in each nanocrystal decrease gradually, which are in consistent with the change trend of d-spacing values of (200) plane obtained from powder XRD patterns.

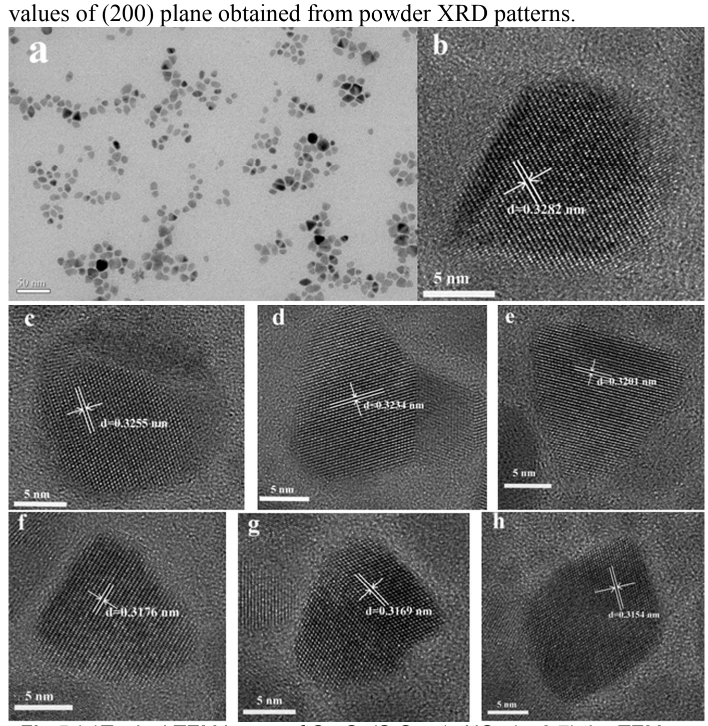

Fig.5 (a)Typical TEM image of $Cu_2Sn(S_xSe_{1-x})_3$ NCs (x=0.7),the TEM images of the else compositions are shown in FigureS6 (Supporting Information); (b-h) HRTEM image of the $d_{(200)}$ lattice fringes for $Cu_2Sn(S_xSe_{1-x})_3$ nanocrystals with (b) x=0, (c) x=0.2, (d) x=0.3, (e) x=0.5, (f) x=0.7, (g) x=0.8, (h) x=1.

The UV-vis-NIR absorption spectra of the $Cu_2Sn(S_xSe_{1-x})_3$ NCs was measured to study their optical properties. The band gap energies (E_g) were determined by extrapolating straight line of the plot $(\alpha h\upsilon)^2$ *versus* $h\upsilon$ to intercept the x abscissa (Figure 6（a）). To further understand the relation between the alloy composition and their band gap evolution, the band gaps of the nanocrystals were plotted as a function of x (Figure 6 (b)). It was found that the optical band gap of samples shows a curve, which is termed as band gap “bowing”. The data points were fitted by the modified bowing equation as follows:

$$E_g(x) = xE_g^{Cu_2SnS_3} + (1-x)E_g^{Cu_2SnSe_3} - x(1-x)/b$$

Where $E_g^{Cu_2SnS_3}$ and $E_g^{Cu_2SnSe_3}$ are the bandgaps of Cu_2SnS_3 and Cu_2SnSe_3, respectively; b is the bowing parameter describing the nonlinear relationship between band gap and composition. The bowing parameter determined by the best fitting curve is 0.12 eV, which slightly deviates from the linear relation and shows a nonlinear dependence of band gap and x in $Cu_2Sn(S_xSe_{1-x})_3$ nanocrystals. This nonlinear relation has been reported in literatures and could possibly result of several effects: (i) band-structure variations resulting from the alternating lattice constant, (ii) electron distribution deformation resulting from the difference in electronegativity among the atoms, and (iii) differently sized constituents resulting from the internal structural relaxation of the anion–cation bond lengths and angles.[6, 10]

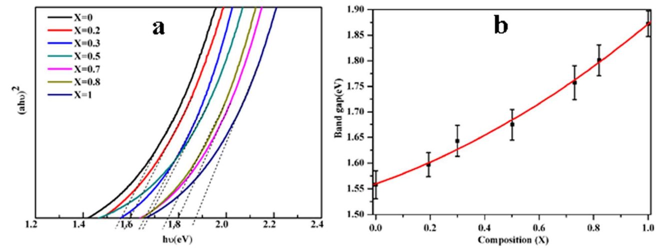

Fig.6 (a) An extrapolation of the spectra to identify the band edge of $Cu_2Sn(S_xSe_{1-x})_3$ nanocrystals for various values of x; (b) optical band gap of $Cu_2Sn(S_xSe_{1-x})_3$ nanocrystals as a function of x.

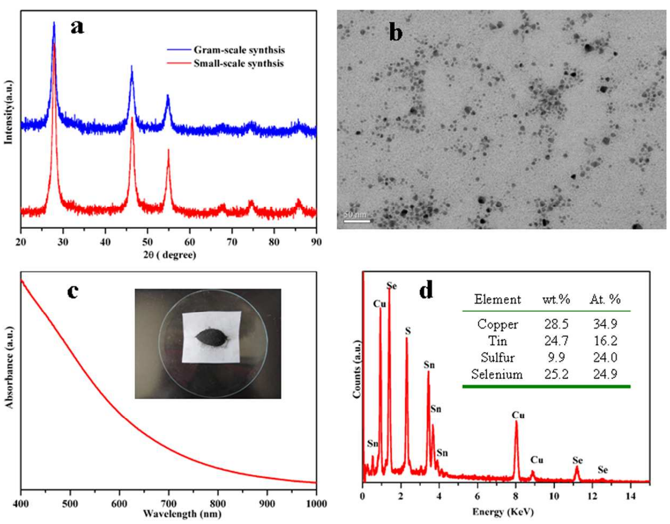

Fig.7 $Cu_2Sn(S_{0.5}Se_{0.5})_3$ NCs prepared by a large-scale procedure. (a) XRD patterns of gram-, and small-scale synthesis; (b) TEM image; (c) the UV-vis absorption spectrum, the inset shows the obtained 2.0746 g dried $Cu_2Sn(S_{0.5}Se_{0.5})_3$ NCs powders; (d) Element composition of a field of $Cu_2Sn(S_{0.5}Se_{0.5})_3$ nanocrystals measured by EDS, inset: the quantitative elemental analysis results.

This one-spot synthesis does not require precursor injection and relies on relatively inexpensive, environmentally friendly reagents. The heating method present here can provide a facile route for large-scale and high-throughput production of $Cu_2Sn(S_xSe_{1-x})_3$ NCs. To test the up-scaling, we increase the synthesis to 10-fold of the volume compared to that in the syntheses discussed in the previous sections. Figure 7 depicts the results of a typical gram-scale synthesis, by decomposition of 10 mmol $Cu(OAc)_2$, 5 mmol $SnBr_2$, 7.5 mmol Se and 7.5 mmol S in a 100 mL flask containing of 60 mL oleylamine and 6 mL 1-dodecanethiol at 240 °C. The heating time was again keeping for 1 h. The XRD pattern confirms that NCs obtained from the scale-up procedure have the same crystal structure with the small-scale synthesis, with no other phases and side products. EDS of a field of nanocrystals indicates that the average Cu:Sn:S:Se molar ratio is 2.1:1:1.48:1.52, matching greatly well with the precursor molar ratio (2:1:1.5:1.5). The average diameter of the nanoparticles synthesized by the up-scale procedure is slightly smaller than that of the small-scale synthesis, as shown in the XRD and TEM. This is due to the fact that the precursor concentration in the up-scale procedure is slightly higher, and the high precursor concentration usually results in small nanoparticles. These as-prepared nanocrystals can also be dispersed in most organic solvents and possess good colloidal stability in solution for several months.

The chemical yield is an important aspect for the large-scale synthesis. It can be estimated from a comparison of the total weight of the product and that of the initial precursors. To calculate the synthesis yield, the contribution of the residual solvent and organic ligand to the weight of the final product was estimated from TGA analysis (Figure S 7), and a synthesis yield of 93% was found. We can therefore conclude that the present synthesis approach could be utilized to produce large quantities of stoichiometry-controlled $Cu_2Sn(S_xSe_{1-x})_3$ nanocrystals.

To validate the optoelectronic properties of the as-large-scale synthesized $Cu_2Sn(S_{0.5}Se_{0.5})_3$ nanocrystals, the current–voltage (I–V) measurements for the $Cu_2Sn(S_{0.5}Se_{0.5})_3$ thin films were performed. The film was fabricated on patterned indium tin oxide (ITO)-coated glass substrate via spin-casting using a toluene solution of $Cu_2Sn(S_{0.5}Se_{0.5})_3$ NCs. After that, the aluminum (Al) cathode with 100 nm thick was deposited by thermal evaporation. Figure S 8 shows the I–V curves of the $Cu_2Sn(S_{0.5}Se_{0.5})_3$ film tested in the dark and under an illumination intensity of 100 mW cm^{-2}, which was measured in a 1 V bias range. The device exhibits a strong increase in current under light irradiation in comparison to the dark state. Light irradiation excites electrons in the valance band to the conduction band and then increases the holes in the $Cu_2Sn(S_{0.5}Se_{0.5})_3$. As a result, the current is increased obviously and the conductivity of the film is enhanced. The obvious photoresponsive behavior suggests that the as-synthesized $Cu_2Sn(S_{0.5}Se_{0.5})_3$ will be a potential candidate in the fabrication of photovoltaic devices.

These nanocrystals are potential materials used for photovoltaic absorber film fabrication, but a ligand exchange procedure that frees the NCs from carbon-containing stabilizers and property comparison between nanocrystals and films prepared by these nanocrystals still require further study.

Conclusions

In summary, we have reported a facile, green heating procedure for the synthesis of multicomponent $Cu_2Sn(S_xSe_{1-x})_3$ nanocrystals. By modulating the precursor molar ratios, the composition of the resultant NCs could be tuned over the whole range, from Cu_2SnS_3 to Cu_2SnSe_3. The lattice parameters (a and c) of the $Cu_2Sn(S_xSe_{1-x})_3$ NCs were consistent with Vegard's law, which confirmed the formation of homogeneous nanocrystals. The XRD and TEM results indicated that the as-prepared $Cu_2Sn(S_xSe_{1-x})_3$ NCs have the monoclinic structure. The band gap of the $Cu_2Sn(S_xSe_{1-x})_3$ NCs could be tailored from 1.55 to 1.87 eV by decreasing the Se content, yielding a nonlinear relation with x having a bowing constant of 0.12 eV. By scaling up the amount of precursors 10-fold using the same synthesis scheme, gram-scale amounts of $Cu_2Sn(S_{0.5}Se_{0.5})_3$ NCs could be collected, which was facilitated by the high chemical yield of the synthesis(93%), while still maintaining control over the phase and composition. The photoresponsive behavior indicates the potential use of as-large-scale synthesized $Cu_2Sn(S_{0.5}Se_{0.5})_3$ nanocrystals in solar energy conversion systems.Given the general approach in terms of precursors, solvents, and temperatures used, our strategy might be suitable for large-scale synthesis of nanomaterials for low-cost photovoltaics.

Acknowledgements

This work was supported by the National Natural Science Foundation of China under grants no. 20871023, 51002148, 21071141, and 20921002.

Notes and references

[1]*State Key Laboratory of Rare Earth Resources Utilization, Changchun Institute of Applied Chemistry, Chinese Academy of Sciences, Changchun 130022, P. R. China*
[2]College of Chinese Academy of Sciences, Beijing 10049, P. R. China
Electronic Supplementary Information (ESI) available. See DOI: 10.1039/b000000x/

1. Z. B. Haizheng Zhong, and Bingsuo Zou, *J. Phys. Chem. Lett.*, 2012, **3**, 3167-3175.
2. E. Witt and J. Kolny-Olesiak, *Chemistry*, 2013.
3. D. Y. Yi Liu, † Liang Shen,‡ Hao Zhang,*,† Xindong Zhang,‡ and Bai Yang†, *J. Am. Chem. Soc.*, 2012, **134**, 7207-7210.
4. M. Altosaar, J. Raudoja, K. Timmo, M. Danilson, M. Grossberg, J. Krustok and E. Mellikov, *physica status solidi (a)*, 2008, **205**, 167-170.
5. S. C. Riha, B. A. Parkinson and A. L. Prieto, *J Am Chem Soc*, 2011, **133**, 15272-15275.
6. H. Wei, Z. Ye, M. Li, Y. Su, Z. Yang and Y. Zhang, *CrystEngComm*, 2011, **13**, 2222.
7. M. Grossberg, J. Krustok, J. Raudoja and T. Raadik, *Applied Physics Letters*, 2012, **101**, 102102.
8. F. J. Fan, Y. X. Wang, X. J. Liu, L. Wu and S. H. Yu, *Adv Mater*, 2012, **24**, 6158-6163.
9. F.-J. Fan, L. Wu and S.-H. Yu, *Energy & Environmental Science*, 2014, **7**, 190.
10. K.-L. Ou, J.-C. Fan, J.-K. Chen, C.-C. Huang, L.-Y. Chen, J.-H. Ho and J.-Y. Chang, *J Mater Chem*, 2012, **22**, 14667.
11. S. Chen, A. Walsh, X. G. Gong and S. H. Wei, *Adv Mater*, 2013, **25**, 1522-1539.
12. Y.-T. Zhai, S. Chen, J.-H. Yang, H.-J. Xiang, X.-G. Gong, A. Walsh, J. Kang and S.-H. Wei, *Phys Rev B*, 2011, **84**.
13. J. Jeong, H. Chung, Y. C. Ju, J. Moon, J. Roh, S. Yoon, Y. R. Do and W. Kim, *Materials Letters*, 2010, **64**, 2043-2045.
14. M. E. Norako, M. J. Greaney and R. L. Brutchey, *J Am Chem Soc*, 2012, **134**, 23-26.
15. M. Ahmadi, S. S. Pramana, S. K. Batabyal, C. Boothroyd, S. G. Mhaisalkar and Y. M. Lam, *Inorg Chem*, 2013, **52**, 1722-1728.
16. M. Ibáñez, D. Cadavid, U. Anselmi-Tamburini, R. Zamani, S. Gorsse, W. Li, A. M. López, J. R. Morante, J. Arbiol and A. Cabot, *Journal of Materials Chemistry A*, 2013, **1**, 1421.
17. T. Nomura, T. Maeda, K. Takei, M. Morihama and T. Wada, *physica status solidi (c)*, 2013, n/a-n/a.
18. J. Koike, K. Chino, N. Aihara, H. Araki, R. Nakamura, K. Jimbo and H. Katagiri, *Japanese Journal of Applied Physics*, 2012, **51**, 10NC34.
19. D. M. Berg, R. Djemour, L. Gütay, G. Zoppi, S. Siebentritt and P. J. Dale, *Thin Solid Films*, 2012, **520**, 6291-6294.
20. J. Wang, A. Singh, P. Liu, S. Singh, C. Coughlan, Y. Guo and K. M. Ryan, *J Am Chem Soc*, 2013.
21. S. W. Shin, J. H. Han, Y. C. Park, G. L. Agawane, C. H. Jeong, J. H. Yun, A. V. Moholkar, J. Y. Lee and J. H. Kim, *J Mater Chem*, 2012, **22**, 21727.
22. Y. Cao, M. S. Denny, J. V. Caspar, W. E. Farneth, Q. Guo, A. S. Ionkin, L. K. Johnson, M. Lu, I. Malajovich, D. Radu, H. D. Rosenfeld, K. R. Choudhury and W. Wu, *Journal of the American Chemical Society*, 2012, **134**, 15644-15647.
23. C. Yang, B. Zhou, S. Miao, C. Yang, B. Cai, W. H. Zhang and X. Xu, *J Am Chem Soc*, 2013.
24. M. R. Renguo Xie, and Xiaogang Peng*, *J. AM. CHEM. SOC.*, 2009, **131**, 5691–5697.
25. J. Feng, M. Sun, F. Yang and X. Yang, *Chemical Communications*, 2011, **47**, 6422.
26. S.-H. C. Ming-Yi Chiang, † Chia-Yu Chen, Fang-Wei Yuan, and Hsing-Yu Tuan*, *J. Phys. Chem. C*, 2011, **115**, 1592–1599.
27. M. Ibáñez, D. Cadavid, R. Zamani, N. García-Castelló, V. Izquierdo-Roca, W. Li, A. Fairbrother, J. D. Prades, A. Shavel, J. Arbiol, A. Pérez-Rodríguez, J. R. Morante and A. Cabot, *Chemistry of Materials*, 2012, **24**, 562-570.
28. M. Ibanez, R. Zamani, A. LaLonde, D. Cadavid, W. Li, A. Shavel, J. Arbiol, J. R. Morante, S. Gorsse, G. J. Snyder and A. Cabot, *J Am Chem Soc*, 2012, **134**, 4060-4063.
29. E. Dilena, Y. Xie, R. Brescia, M. Prato, L. Maserati, R. Krahne, A. Paolella, G. Bertoni, M. Povia, I. Moreels and L. Manna, *Chemistry of Materials*, 2013, 130724141635003.
30. P. M. A. a. M. G. Bawendi*, *J. AM. CHEM. SOC.*, 2008, **130**, 9240–9241.
31. R. N. P. Bonil Koo, and Brian A. Korgel*, *J. AM. CHEM. SOC.*, 2009, **131**, 3134–3135.
32. M. Ibáñez, R. Zamani, W. Li, A. Shavel, J. Arbiol, J. R. Morante and A. Cabot, *Crystal Growth & Design*, 2012, **12**, 1085-1090.
33. L. Li, A. Pandey, D. J. Werder, B. P. Khanal, J. M. Pietryga and V. I. Klimov, *Journal of the American Chemical Society*, 2011, **133**, 1176-1179.
34. A. Shavel, D. Cadavid, M. Ibanez, A. Carrete and A. Cabot, *J Am Chem Soc*, 2012, **134**, 1438-1441.
35. T. J. D. Liang Li, ‡,§ Isabelle Texier,‡ Tran Thi Kim Chi,| Nguyen Quang Liem,| and and Peter Reiss*, *Chem. Mater.*, 2009, **21**, 2422–2429.
36. T. P. E. Cassette, *,† C. Bouet,† M. Helle,‡ L. Bezdetnaya,‡ F. Marchal,‡ and and B. Dubertret†, *Chem. Mater.*, 2010, **22**, 6117–6124.

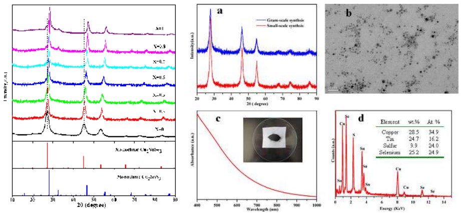

A facile, low-cost synthesis of compositionally tunable $Cu_2Sn(S_xSe_{1-x})_3$ colloidal nanocrystals was reported, and the scalable procedure is also provided .